PERGAMON

International Journal of Solids and Structures 40 (2003) 5949–5972

INTERNATIONAL JOURNAL OF SOLIDS and STRUCTURES

www.elsevier.com/locate/ijsolstr

# SMA-induced snap-through of unsymmetric fiber-reinforced composite laminates

M.-L. Dano [a,1], M.W. Hyer [b,*]

[a] Département de Genie Mécanique, Université LAVAL, Pavillon Adrien-Pouliot Québec, Que., Canada G1K 7P4
[b] Department of Engineering Science and Mechanics, Virginia Polytechnic Institute and State University, Blacksburg, VA 24061, USA

Received 10 February 2003

**Abstract**

A theory is developed and experiments designed to study the concept of using shape memory alloy (SMA) wires to effect the snap-through of unsymmetric composite laminates. The concept is presented in the context of structural morphing, that is, a structure changing shape to adjust to changing conditions or to change operating characteristics. While the specific problem studied is a simplification, the overall concept is to potentially take advantage of structures which have multiple equilibrium configurations and expend power only to change the structure from one configuration to another rather than to continuously expend power to hold the structure in the changed configuration. The unsymmetric laminate could be the structure itself, or simply part of a structure. Specifically, a theory is presented which allows for the prediction of the moment levels needed to effect the snap-through event. The moment is generated by a force and support arrangement attached to the laminate. A heated SMA wire attached to the supports provides the force. The necessary SMA constitutive behavior and laminate mechanics are presented. To avoid dealing with the heat transfer aspects of the SMA wire, the theory is used to predict snap-through as a function of SMA wire temperature, which can be measured directly. The geometry and force level considerations of the experiment are discussed, and the results of testing four unsymmetric laminates are compared with predictions. Laminate strain levels vs. temperature and the snap-through temperatures are measured for the these laminates. Repeatability of the experimental results is generally good, and the predictions are in reasonable agreement with the measurements.


*Keywords:* Thermally-induced deformations; Stability; Geometrically nonlinear effects; Rayleigh–Ritz technique

## 1. Introduction and background

Unsymmetrically laminated fiber-reinforced polymer matrix composite laminates provide a number of interesting characteristics for discussions regarding multiple equilibrium configurations, structural stability,

* Corresponding author. Tel.: +1-540-231-5372; fax: +1-540-231-4574.
*E-mail addresses:* mldano@gmc.ulaval.ca (M.-L. Dano), hyerm@vt.edu (M.W. Hyer).
[1] Tel.: +1-418-656-2242; fax: +1-418-656-7415.


doi:10.1016/S0020-7683(03)00374-3

and the ability to design shape into a structure. For example, an eight-layer $[90_4/0_4]_T$ laminate that is flat at its elevated cure temperature, as in Fig. 1a, cools from its cure temperature to have two equilibrium configurations. One configuration is cylindrical and has a large curvature in the $x$-direction and an imperceptible curvature in the $y$-direction, Fig. 1b. The other configuration is cylindrical and has a large curvature in the $y$-direction and an imperceptible curvature in the $x$-direction, Fig. 1c. The curvatures for the two configurations are equal but of opposite signs, and the laminate can be changed from one configuration to the other by a simple snap-through action initiated by applying equal and opposite moments to the edges of the laminate. Analysis indicates there is a third equilibrium configuration that is saddle-

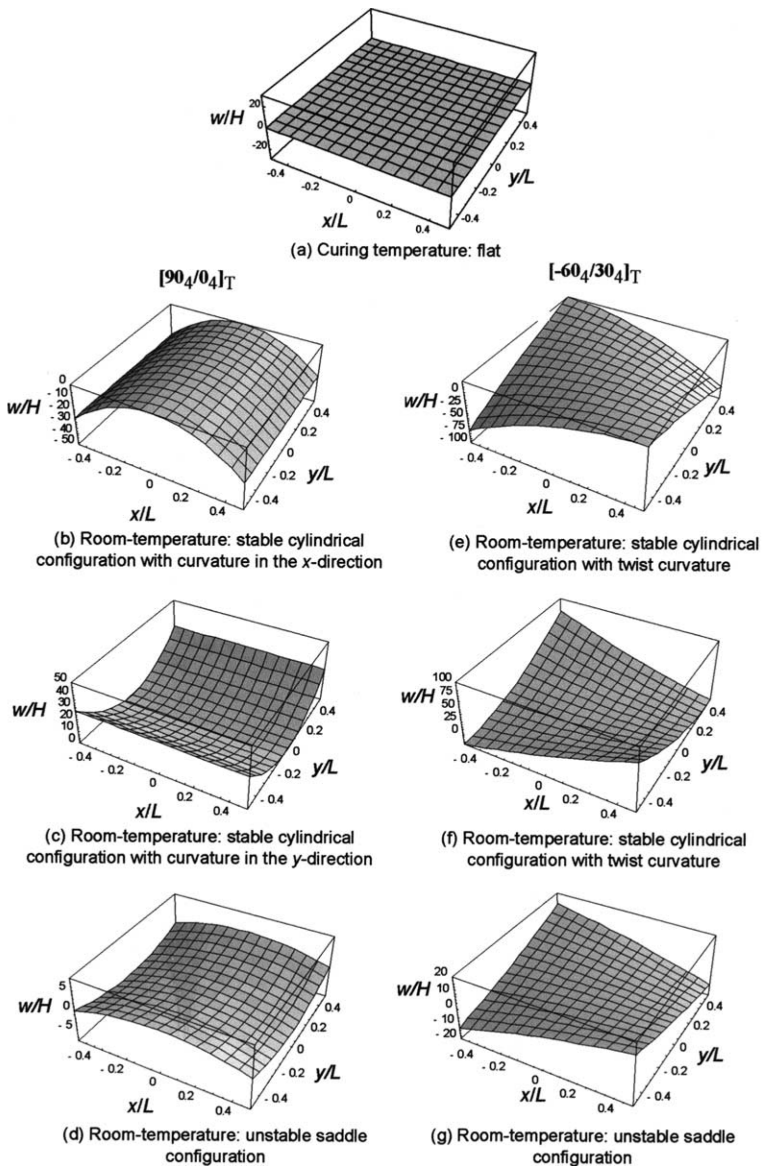


Fig. 1. Shapes of $[90_4/0_4]_T$ and $[-60_4/30_4]_T$ laminate.

shaped, as in Fig. 1d. A stability investigation indicates the saddle is not stable, while both of the cylindrical configurations are stable. Both cylindrical configurations have the same total potential energy, so each one is as likely to exist as the other, and only small imperfections in the laminate will favor one configuration relative to the other. A $[-60_4/30_4]_T$ laminate, shown on the right side of Fig. 1, will have similar characteristics. However, because of the off-axis nature of the fiber orientations, the cooled laminate will have twist curvature, and the principal curvature directions will not be aligned with the $x$- and $y$-coordinate axes. While these characteristics of unsymmetrically laminated composite materials are quite interesting, modeling can become involved and traditional analysis methods, like finite-element analysis, have difficulty with the multiple equilibrium configurations and the inherent instability in the problem. Dano and Hyer (1997) expanded on the earlier work of Hyer (1981a,b, 1982) and Hamamoto and Hyer (1987) to study several families of unsymmetric laminates both experimentally and with a semi-closed form energy-based Rayleigh–Ritz predictive technique. Schlecht et al. (1995) and Schlecht and Schulte (1999) used finite-elements to study the interesting characteristics of unsymmetric laminates. Others have also investigated their behavior, namely, Jun and Hong (1990, 1992), Peeters et al. (1996), Tuttle et al. (1996), and Cho et al. (1998).

The idea of being able to apply moments to the laminate and change the laminate to a significantly different equilibrium configuration is intriguing. In the areas of structural morphing and so-called smart structures, actuators are used to force a structure from one configuration to another to react to the environment or to change the operating characteristics of the structure. However, most smart structure concepts require the continuous application of a force, at the expense of a continuous source of energy, to cause a structure to maintain a changed configuration. With the use of unsymmetric laminates, it might be possible to use the multiple equilibrium configurations to advantage. The unsymmetric laminate could be the structure itself, or it could be part of a structure, and energy would be expended only to change the structure from one configuration to the other. A continuous supply of energy would not be required. Two important issues with this concept are the method of actuation, and the force, or moment, levels required. This paper addresses these issues. The approach in the paper is rather basic and not one that explores all options or answers all questions. Rather, the paper presents an idea, develops a theory to make predictions based on the idea, and presents the results of experiments designed to further explore the concept. Specifically, this paper explores the notion of using shape memory alloy (SMA) wires to effect the snap-through from one stable configuration to the other. As a moment requires both a force and a moment arm, there is some flexibility regarding how this can be accomplished. The concept to be discussed in the present paper is illustrated in Fig. 2. There the $[-60_4/30_4]_T$ laminate in the cylindrical configuration of Fig. 1e is shown outfitted with supports of length $e$ attached. A SMA wire is stretched between the tips of the supports. It is assumed that the wire has been pre-strained and is in the martensite phase. It is further assumed that the wire is then heated and is transformed to the austenite phase, whereupon it has the tendency to return to the length it had before prestraining, and does so by generating enough force to pull the tips of the supports

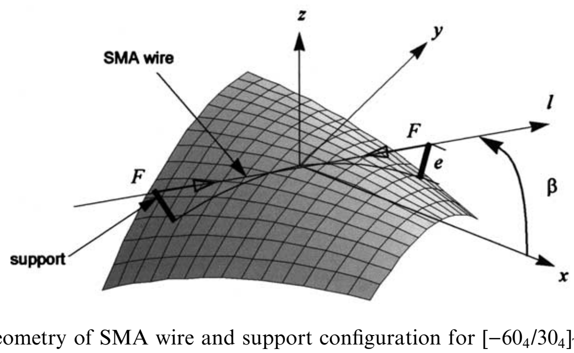


Fig. 2. Geometry of SMA wire and support configuration for $[-60_4/30_4]_T$ laminate.

towards each other, thereby creating the equal and opposite moments needed to cause the laminate to snap. As the laminate deforms toward the snapping condition, the tips of the supports move due to the translations and rotations of the laminate at the base of the supports, but the line of action of the force is always directed along the line connecting the tips. The supports are mounted so that, initially, the line of action between the supports, denoted as the $l$-axis in Fig. 2, is along the principal curvature direction. As the laminate deforms, however, the line of action changes. Of course, to effect the reverse snap, a similar arrangement of supports and SMA wire would be needed on the underside of the laminates. The support scheme shown in Fig. 2, along with the accompanying supports on the underside, raises a number of questions. First, the arrangement seems untidy, perhaps even cumbersome. With the arrangement shown, the first thought is that the length $e$ of the supports should probably be long enough that the SMA wire does not touch the laminate at the center. Long supports contribute to the untidiness. Long supports may not be necessary, however. Perhaps a series of shorter supports could be used so the SMA wire would more closely follows the contour of the curved laminate, elevated from the surface of the laminate, not touching it. It might even be possible to bond the SMA wire to the surface of the laminate, or embed it within the laminate, thus making the concept more streamlined and less obtrusive. With the concept shown in Fig. 2, or with any of these alternative concepts, the factors that have to be considered are: the force level that can be generated with SMA wire; the moment level needed to produce snapping; the recovery strain levels in the SMA wire; and the geometry of the set-up. These issues are all coupled with the effects of fiber orientations within the unsymmetric laminate, as 'less' unsymmetric laminates require less of a moment to cause snapping, have less of a chance of causing the wire to reach the recovery strain or force limits of the SMA wire, and have less curvature, thereby simplifying the geometry of the set-up. Additionally, the SMA wire must be heated and the parameters associated with this heating, namely, the voltage drop along the wire, the current through the wire, the wire temperature, and heat transfer from the wire must be considered. These considerations all depend on the conditions surrounding the wire, the diameter of the wire, the length of wire, and a number of other variables. The simple arrangement shown in Fig. 2 was chosen for this initial study so that there were fewer variables to consider, experiments could be done easier, and the basic concept was verified. The basic objective of the study was to be able to predict the deformation of the laminate, and in particular, the snap-through event, as a function of the temperature of the SMA wire. The wire was heated by passing current through it, and the concerns for voltage and current levels needed, heat transfer effects, etc. were not addressed.

In the sections to follow, the method of predicting the deformation of an unsymmetric laminate to forces in the arrangement shown in Fig. 2 is outlined. The method is based on the Rayleigh–Ritz technique, whereby the functional form of the laminate displacements is assumed. This has been discussed in Dano and Hyer (1996, 2002) but, for purposes of completeness, it is felt necessary to briefly review those steps here. Following that, the characteristics of SMA wire as they apply to the current problem are reviewed, and the equations governing wire behavior, which were adapted from the work of other researchers, presented. The equations governing laminate behavior are then coupled to the equations governing SMA wire behavior and the computation scheme to predict laminate shape as function of wire temperature is outlined. Experiments are then described that are used to calibrate the computational scheme, using a flat aluminum plate, and to examine the deformation and snap-through characteristics of four unsymmetric laminates. The outcome of the experiments and the predictions of the computational scheme are compared.

## 2. Review of theory to predict snap-through forces

A planform view of the geometry locating the base of the supports is shown in Fig. 3a. The angle $\Phi_0$ is the angle the principal curvature direction makes with the $+x$-axis of the laminate before any forces are applied. The geometric quantities in Fig. 3a are related by

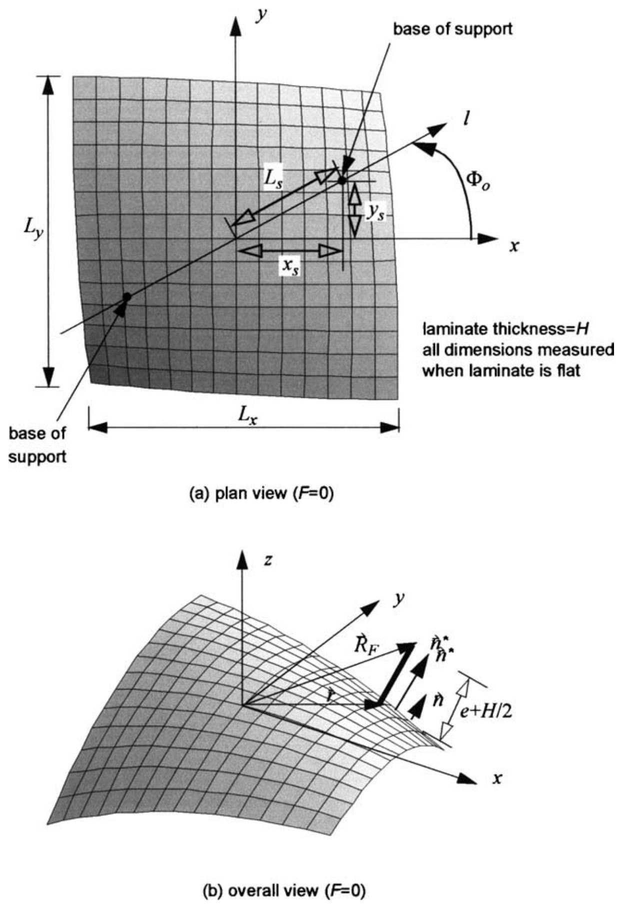


Fig. 3. Geometry of the force configuration.

$$x_s = L_s \cos \Phi_0, \qquad y_s = L_s \sin \Phi_0, \tag{1}$$

where $L_s$, $x_s$, and $y_s$ are measured when the laminate is flat. The response of the laminate to the SMA-induced forces is determined using the principle of virtual work, which can be stated as

$$\delta W_T = \delta \Pi - \delta W_F = 0, \tag{2}$$

where $\delta W_T$ is the total virtual work, $\delta \Pi$ the first variation of the strain energy, and $\delta W_F$ the virtual work of the applied forces. Assuming classical lamination theory is valid (Hyer, 1998), the strain energy of the laminate, $\Pi$, can be expressed as a function of the material and geometric properties of the laminate, the temperature change of the laminate relative to the cure temperature, $\Delta T$, and the total strains by,

$$\begin{aligned}\Pi = \int_{-L_x/2}^{L_x/2}\int_{-L_y/2}^{L_y/2}\int_{-H/2}^{H/2} \bigg( & \frac{1}{2}\overline{Q}_{11}\varepsilon_x^2 + \overline{Q}_{12}\varepsilon_x\varepsilon_y + \overline{Q}_{16}\gamma_{xy}\varepsilon_x + \frac{1}{2}\overline{Q}_{22}\varepsilon_y^2 + \overline{Q}_{26}\gamma_{xy}\varepsilon_y + \frac{1}{2}\overline{Q}_{66}\gamma_{xy}^2 \\ & - (\overline{Q}_{11}\alpha_x + \overline{Q}_{12}\alpha_y + \overline{Q}_{16}\alpha_{xy})\varepsilon_x\Delta T - (\overline{Q}_{12}\alpha_x + \overline{Q}_{22}\alpha_y + \overline{Q}_{26}\alpha_{xy})\varepsilon_y\Delta T \\ & - (\overline{Q}_{16}\alpha_x + \overline{Q}_{26}\alpha_y + \overline{Q}_{66}\alpha_{xy})\gamma_{xy}\Delta T \bigg)\,dx\,dy\,dz, \end{aligned} \tag{3}$$

where the $Q_{ij}$s are the transformed reduced stiffnesses of the individual layers, $L_x$ and $L_y$ are the planform dimensions of the laminate when it is flat, and $H$ is the laminate thickness. The total strains $\varepsilon_x$, $\varepsilon_y$, $\gamma_{xy}$ are given by the Kirchhoff hypothesis as

$$\varepsilon_x = \varepsilon_x^0 + z\kappa_x^0, \qquad \varepsilon_y = \varepsilon_y^0 + z\kappa_y^0, \qquad \gamma_{xy} = \gamma_{xy}^0 + z\kappa_{xy}^0, \tag{4}$$

where the quantities $\varepsilon_x^0$, $\varepsilon_y^0$, $\gamma_{xy}^0$ and $\kappa_x^0$, $\kappa_y^0$, $\kappa_{xy}^0$ are the total midplane strains and curvatures, respectively, defined by

$$\begin{aligned}
&\varepsilon_x^0 = \frac{\partial u^0}{\partial x} + \frac{1}{2}\left(\frac{\partial w^0}{\partial x}\right)^2, \qquad \varepsilon_y^0 = \frac{\partial v^0}{\partial y} + \frac{1}{2}\left(\frac{\partial w^0}{\partial y}\right)^2,\\
&\gamma_{xy}^0 = \frac{\partial u^0}{\partial y} + \frac{\partial v^0}{\partial x} + \frac{\partial w^0}{\partial x}\frac{\partial w^0}{\partial y},\\
&\kappa_x^0 = -\frac{\partial^2 w^0}{\partial x^2}, \qquad \kappa_y^0 = -\frac{\partial^2 w^0}{\partial y^2}, \qquad \kappa_{xy}^0 = -2\frac{\partial^2 w^0}{\partial x \partial y}.
\end{aligned} \tag{5}$$

The displacements can be assumed to be of the form

$$\begin{aligned}
&u^0(x,y) = c_1 x + c_{12} y + \frac{1}{2}\left(c_4 - \frac{1}{2}c_9 c_{11}\right)x^2 y + \left(c_3 - \frac{c_{11}^2}{8}\right)xy^2 + \frac{1}{3}\left(c_2 - \frac{1}{2}c_9^2\right)x^3 + \frac{1}{3}c_{13}y^3,\\
&v^0(x,y) = c_{12} x + c_5 y + \left(c_6 - \frac{c_{11}^2}{8}\right)x^2 y + \frac{1}{2}\left(c_8 - \frac{1}{2}c_{10}c_{11}\right)xy^2 + \frac{1}{3}\left(c_7 - \frac{1}{2}c_{10}^2\right)y^3 + \frac{1}{3}c_{14}x^3,\\
&w^0(x,y) = \frac{1}{2}\left(c_9 x^2 + c_{10} y^2 + c_{11} xy\right),
\end{aligned} \tag{6}$$

where $u^0$, $v^0$, and $w^0$ are the displacement components in the $x$-, $y$- and $z$-directions, respectively, and the $c_i$, $i = 1, \ldots, 14$ are constants that are determined by enforcement of Eq. (2). Substituting Eqs. (4)–(6) into Eq. (3) results in an expression for the strain energy of the laminate of the form

$$\Pi = \Pi(c_i, i = 1, \ldots, 14). \tag{7}$$

Obviously, $\Pi$ is also a function of the laminate material properties, geometry, and temperature change, but here interest centers on its dependence on the unknown coefficients. From Eq. (7), the first variation of the strain energy can be expressed as

$$\delta\Pi = \delta\Pi(c_1, c_2, \ldots, \delta c_1, \delta c_2, \ldots). \tag{8}$$

Referring to Fig. 3b, the virtual work of the applied force $\vec{F}$ is defined as the work done by the force as the laminate is given a virtual displacement, that is,

$$\delta W_F = \vec{F} \cdot \delta\vec{R}_F\Big|_{\substack{x=x_s\\ y=y_s}} + \vec{F} \cdot \delta\vec{R}_F\Big|_{\substack{x=-x_s\\ y=-y_s}}. \tag{9}$$

The virtual displacement $\delta\vec{R}_F$ is evaluated by first computing the position vector $\vec{R}_F$ of the force, relative to the origin of the coordinate system, and then taking its variation. As illustrated in Fig. 3b, the position vector $\vec{R}_F$ can be expressed as the sum of the position vector to the base of the support, $\vec{r}$, and the vector directed from the base of the support to the tip of the support, $\vec{n}^*$, i.e.,

$$\vec{R}_F = \vec{r} + \vec{n}^*. \tag{10}$$

The vector $\vec{r}$ can be written as

$$\vec{r} = (x + u^0(x, y, c_i, i = 1, \ldots, 14))\vec{i} + (y + v^0(x, y, c_i, i = 1, \ldots, 14))\vec{j} + w^0(x, y, c_i, i = 1, \ldots, 14)\vec{k}, \tag{11}$$

where the notation is to emphasize the fact that the vector $\vec{r}$ depends on the unknown coefficients as well as $x$ and $y$. Since the vector $\vec{n}^*$ is normal to the surface, it can be expressed as

$$\vec{n}^* = \left(e + \frac{H}{2}\right)\vec{n}, \tag{12}$$

where $\vec{n}$ is the unit vector normal to the laminate surface at the support locations and $(e + H/2)$ is the distance from the laminate reference surface to the tip of the support. By definition, the unit vector $\vec{n}$ at a point $(x, y)$ on the laminate surface is given by,

$$\vec{n}(x, y) = \frac{\frac{\partial \vec{r}}{\partial x} \times \frac{\partial \vec{r}}{\partial y}}{\left| \frac{\partial \vec{r}}{\partial x} \times \frac{\partial \vec{r}}{\partial y} \right|}. \tag{13}$$

Because of Eq. (11), $\vec{n}$ is a function of the $c_i$, $i = 1, \ldots, 14$. The virtual displacement $\delta\vec{R}_F$ is given by

$$\delta\vec{R}_F = \delta\vec{r} + \delta\vec{n}^*, \tag{14}$$

where, from Eq. (11),

$$\delta\vec{r} = \sum_{i=1}^{14} \frac{\partial \vec{r}}{\partial c_i} \delta c_i \tag{15}$$

and from Eq. (12)

$$\delta\vec{n}^* = (e + H/2)\delta\vec{n}. \tag{16}$$

From Eq. (13), since $\vec{r}$ is a function of the $c_i$, $\delta\vec{n}$ of the form

$$\delta\vec{n} = \sum_{i=1}^{14} \vec{N}_i \delta c_i, \tag{17}$$

where $\vec{N}_i$ is introduced as shorthand. As a result, using Eqs. (15)–(17), $\delta\vec{R}_F$ can be written as

$$\delta\vec{R}_F = \sum_{i=1}^{14} \left( \frac{\partial \vec{r}}{\partial c_i} + \left(e + \frac{H}{2}\right)\vec{N}_i \right) \delta c_i. \tag{18}$$

The applied force $\vec{F}$ can be expressed in terms of its components in the $x$–$y$–$z$ coordinate system by

$$\vec{F}\Big|_{\substack{x=x_s \\ y=y_s}} = (-F\cos\beta)\vec{i} + (-F\sin\beta)\vec{j}, \qquad \vec{F}\Big|_{\substack{x=-x_s \\ y=-y_s}} = (F\cos\beta)\vec{i} + (F\sin\beta)\vec{j}, \tag{19}$$

where $\cos\beta$ and $\sin\beta$ can be evaluated using the expression for $\vec{R}_F$ given by Eq. (10). Specifically, letting $\vec{e}_l$ define the unit vector along the $l$-axis, then $\vec{e}_l$ can be expressed as a function of $\vec{R}_F$ by

$$\vec{e}_l = \frac{\vec{R}_F(x_s, y_s) - \vec{R}_F(-x_s, -y_s)}{\left|\vec{R}_F(x_s, y_s) - \vec{R}_F(-x_s, -y_s)\right|} = \cos\beta\,\vec{i} + \sin\beta\,\vec{j}, \tag{20}$$

where the vector defined by $\vec{R}_F(x_s, y_s) - \vec{R}_F(-x_s, -y_s)$ represents the vector pointing from the tip of the support at $(-x_s, -y_s)$ to the tip of support at $(x_s, y_s)$. The expressions for $\cos\beta$ and $\sin\beta$ needed in Eq. (19)

can then be deduced from Eq. (20). Eqs. (18)–(20) can then be used to construct $\delta W_F$ as a function of $\delta c_i$ in Eq. (9). With that, the expression for the total virtual work, Eq. (2), is given by

$$\delta W_{\mathrm{T}} = \sum_{i=1}^{14} \frac{\delta \Pi}{\partial c_i} \delta c_i - \delta W_F = \sum_{i=1}^{14} f_i \delta c_i. \tag{21}$$

The laminate is in equilibrium if the total virtual work vanishes, i.e., $\delta W_{\mathrm{T}} = 0$, for every admissible virtual displacement $\delta c_i$, $i = 1, \ldots, 14$. Equating $\delta W_{\mathrm{T}}$ to zero requires

$$f_i = 0, \quad i = 1, \ldots, 14, \tag{22}$$

which represent 14 highly nonlinear algebraic equations in the 14 unknown coefficients $c_i$, $i = 1, \ldots, 14$. By setting the temperature change $\Delta T$ equal to −280 °F and the force $F$ to zero, solving the equilibrium equations expressed by Eq. (22) gives the cured shapes of the laminate at room temperature, as shown in the examples of Fig. 1. By increasing $F$ and keeping $\Delta T$ at −280 °F, the solutions of the equilibrium equations give the configurations of the laminate as it is deformed by the force $F$ at room temperature. In the computation of the equilibrium solution using the Newton–Raphson technique, the Jacobian

$$J = \left[ \frac{\partial f_i}{\partial c_j} \right], \quad i, j = 1, \ldots, 14, \tag{23}$$

is computed for each temperature increment. The equilibrium solution is stable if and only if the matrix $J$ is positive definite. By calculating the eigenvalues of the Jacobian matrix, the stability of the equilibrium solution can be assessed. When one eigenvalue is equal to zero or negative, the matrix is not positive definite and the equilibrium solution is unstable.

### 2.1. Illustrative numerical results

Not being concerned, for the moment, as to how the forces are generated, Figs. 4 and 5 illustrate the relationship between the curvature of a square graphite-epoxy laminate and the applied moment, the magnitude of the moment being given as the product of the force $F$ and the distance $e$. In these figures the laminate has been cooled −280 °F and the properties of a layer are taken to be

$$\begin{aligned} &E_1 = 24.8 \times 10^6 \text{ psi}, \qquad E_2 = 1.270 \times 10^6 \text{ psi}, \qquad G_{12} = 1.030 \times 10^6 \text{ psi}, \\ &\nu_{12} = 0.335, \qquad \alpha_1 = 0.345 \times 10^{-6}\ {}^\circ\mathrm{F}^{-1}, \qquad \alpha_2 = 15.34 \times 10^{-6}\ {}^\circ\mathrm{F}^{-1}. \end{aligned} \tag{24}$$

A layer thickness is assumed to be 0.005 in. and the laminate planform dimensions are $L_x = L_y = 11.5$ in. Two families of laminates are considered in the figures, and Fig. 4 considers the $[(\Theta - 90)_4/\Theta_4]_{\mathrm{T}}$ family, $\Theta = 0°$, 15°, and 30°. The $\Theta = 0°$ case corresponds to the laminate shown on the left side of Fig. 1, and the $\Theta = 30°$ case corresponds to the laminate on the right side. Considering Fig. 4a and b and a moment level of zero, the laminate configuration in Fig. 1b corresponds to point $C$ in the figures, namely large positive curvature in the $x$-direction and little in the $y$-direction. As the applied moment increases from zero, the curvature in the $x$-direction decreases, while the curvature in the $y$-direction basically remains unchanged. At point $G$, the $x$- and $y$-direction curvatures suddenly snap to point $D'$. The configuration at point $D'$ corresponds very closely to the configuration in Fig. 1c, namely large curvature in the $y$-direction, and virtually none in the $x$-direction. If the moment is reduced to zero from $D'$ to $D$, then the configuration at point $D$ is the configuration of Fig. 1c. Note in Fig. 4c that the principal curvature direction of the changing laminate configuration does not change with applied moment level. Note also from Fig. 4 that all laminates in the family, which is essentially a family of cross-ply laminates, require much the same snapping moment level and they maintain their initial principal curvature direction, meaning there is no twist curvature developed in the principal curvature coordinate system associate with the moment-free configuration. These

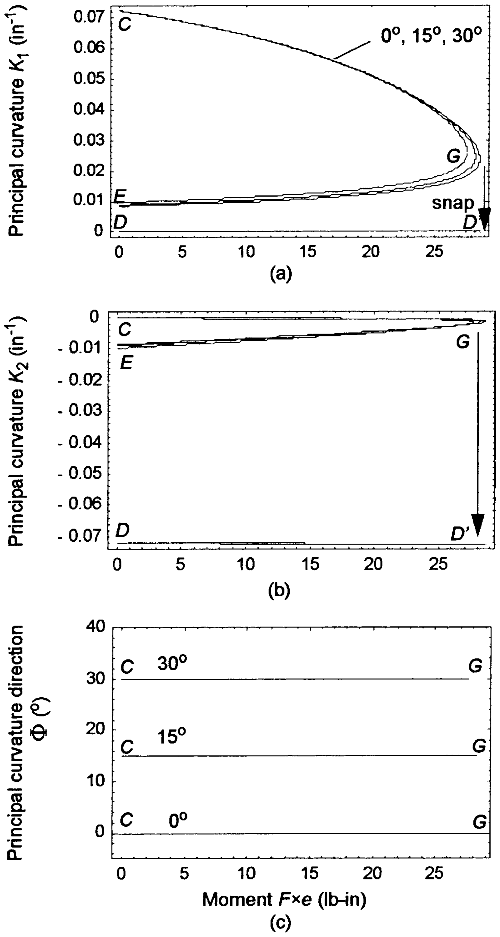


Fig. 4. Moment–deformation relation for $[(\Theta-90)_4/\Theta_4]_T$ laminates.

characteristics are all in contrast to the characteristics of the $[-\Theta_4/\Theta_4]_T$ family, as shown in Fig. 5. For this family the value of $\Theta$ has a strong influence on the moment level required for snapping and the variation of the principal curvature direction with moment level. That the principal curvature direction varies with applied moment level means that as the moment is increased, twist curvature develops in the principal curvature coordinate system associate with the moment-free configuration. The results in Figs. 4 and 5 are important for determining the support geometry and SMA wire scheme used to effect the snap-through. Those issues will be discussed, but first consideration must be given to the SMA wires to be used to generate the moment.

## 3. Use of SMA to generate forces

Since the objective here is to predict the snap-through event of the laminate as a function of the temperature of the SMA wire used to generate the force, a model is needed that relates wire temperature to the force level generated. This is accomplished here by using a constitutive model for SMA wire developed by

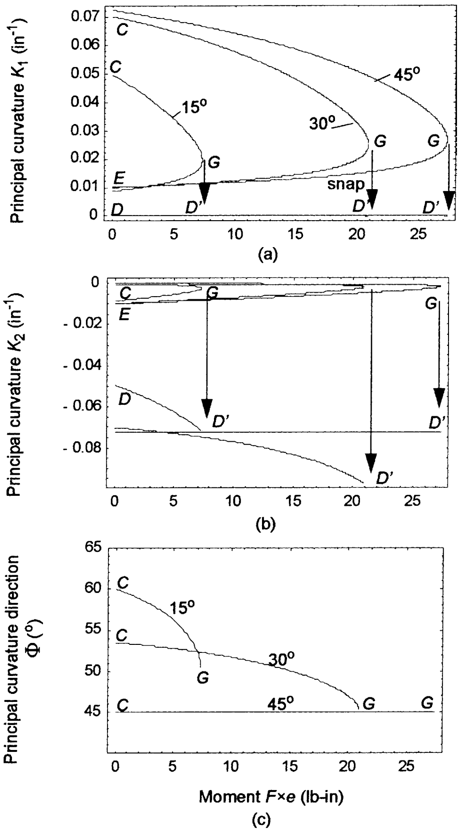


Fig. 5. Moment–deformation relation for $[-\Theta_4/\Theta_4]_T$ laminates.

Boyd and Lagoudas (1996). The model uses a set of equations relating the strain, martensite volume fraction, and temperature in the SMA wire. The constitutive law is a simple generalized Hooke's law, specifically,

$$\sigma = E\varepsilon^e = E(\varepsilon - \varepsilon^t - \alpha(T - T_0)), \tag{25}$$

where, $\sigma$, $\varepsilon^e$, $\varepsilon$, and $\varepsilon^t$ are the uniaxial stress, elastic strain, total strain, and transformation strain, respectively. The quantities $T$ and $T_0$ are, respectively, the present and reference temperature. The extensional modulus $E$ and thermal expansion coefficient $\alpha$ of the SMA wire are both dependent on the martensite volume fraction $\xi$, and are assumed to follow a rule-of-mixtures relationship, namely,

$$E = E_A + \xi(E_M - E_A), \qquad \alpha = \alpha_A + \xi(\alpha_M - \alpha_A), \tag{26}$$

where $E_A$, $\alpha_A$ and $E_M$, $\alpha_M$ are the properties of the SMA in, respectively, a pure austenitic ($A$) and pure martensitic ($M$) phase. The transformation strain $\epsilon^t$ is directly related to the martensite volume fraction by

$$\varepsilon^t = \varepsilon_0\xi, \tag{27}$$

$\varepsilon_0$ being the initial plastic strain in the SMA wire. At $\xi = 1$ the SMA wire is fully martensitic and the transformation strain is equal to the initial strain $\varepsilon_0$. As transformation from the martensitic to the austenitic phases occurs, the initial strain is recovered and therefore strain $\varepsilon^t$ decreases. The constitutive equation, Eq. (25), is used in parallel with a kinetic equation governing the phase transformation which has been derived by using the first and second law of thermodynamics (see Boyd and Lagoudas, 1996, for more details). This kinetic equation can be expressed as

$$\Psi = \sigma^{\mathrm{eff}}\varepsilon_0 + \frac{1}{2}\Delta a^1\sigma^2 + \Delta\alpha\sigma(T - T_0) + \rho\Delta a^4 T - \frac{\partial f(\xi)}{\partial\xi} - Y = 0, \tag{28}$$

where $\rho$ is the SMA density, $\Delta a^1 = 1/E_M - 1/E_A$, $\Delta\alpha = \alpha_M - \alpha_A$, $\sigma^{\mathrm{eff}} = \sigma - \rho b_2\varepsilon^{\mathrm{t}}$, $b_2$ being the kinetic hardening parameter, $\rho\Delta a^4$ is the difference of the entropy between the martensite and the austenite phases at the reference state, $Y$ is the threshold value of transformation, $f(\xi) = (1/2)\rho b_1\xi^2$, $b_1$ being the isotropic hardening parameter. Parameter $b_2$ is assumed to be zero. Parameters $\rho\Delta a^4$, $Y$, and $b_1$ take different values, depending on the direction of the transformation, martensite-to-austenite or austenite-to-martensite. For a martensite-to-austenite transformation,

$$\rho\Delta a^4 = -C_A\varepsilon_0, \qquad Y = -C_A\varepsilon_0 A_{\mathrm{f0}}, \qquad b_1 = \frac{1}{\rho}C_A\varepsilon_0(A_{\mathrm{f0}} - A_{\mathrm{s0}}), \tag{29}$$

whereas for a austenite-to-martensite transformation,

$$\rho\Delta a^4 = -C_M\varepsilon_0, \qquad Y = -C_M\varepsilon_0 M_{\mathrm{s0}}, \qquad b_1 = \frac{1}{\rho}C_M\varepsilon_0(M_{\mathrm{s0}} - M_{\mathrm{f0}}). \tag{30}$$

In the above expressions $M_{\mathrm{s0}}$, $A_{\mathrm{s0}}$, $M_{\mathrm{f0}}$, and $A_{\mathrm{f0}}$ are the start and finish temperatures at zero stress for, respectively, the martensitic and the austenitic transformation. The parameters $C_A$ and $C_M$ are the slopes of the relations between the so-called critical stress and temperature. The stress in the SMA wire should stay within a certain range for a transformation of phase to take place. For transformation to martensite,

$$C_M(T - M_{\mathrm{s0}}) < \sigma < C_M(T - M_{\mathrm{f0}}), \tag{31}$$

and for transformation to austenite,

$$C_A(T - A_{\mathrm{f0}}) < \sigma < C_A(T - A_{\mathrm{s0}}), \tag{32}$$

the expressions on the left and right side of each inequality being referred to as the critical stresses. As shown by the solid line in Fig. 6, as the wire is heated above $A_{\mathrm{s0}}$, the austenitic transformation is initiated and the SMA wire starts recovering strain. As long as the stress $\sigma$ is greater than one critical stress and less than the other critical stress (the two dashed lines in Fig. 6), the transformation and the strain recovery

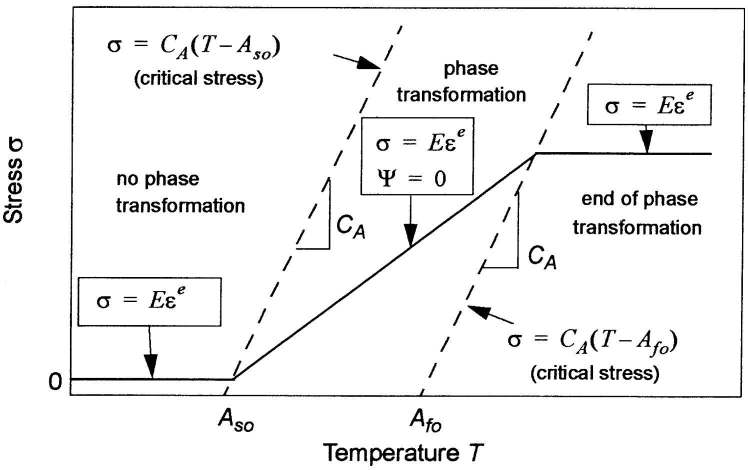


Fig. 6. Stress–temperature relation of SMA.

processes continue. As the stress reaches the critical value, the transformation ends and the recovery process is terminated, even though the initial strain may not be totally recovered. As the phase transformation from martensite to austenite is the transformation of interest here, Eq. (32) gives the effective stress range and the use of Eq. (28) is valid only in this stress interval.

Substituting Eqs. (25) and (27) into Eq. (28) leads to a nonlinear algebraic equation expressed in terms of variables $\varepsilon$, $T$, and $\xi$, namely,

$$\Psi = \Psi(\varepsilon, T, \xi) = 0. \tag{33}$$

The thermomechanical response of the SMA wire can be characterized by solving Eq. (33), which relates the strain and the martensite volume fraction at a given temperature. It is through the strain in Eq. (33), and also the stress by virtue of Eq. (25), that the mechanics of the unsymmetric laminate enter. Essentially, the thermomechanical behavior of the wire and the mechanics of the unsymmetric laminate are coupled through the movement of the supports and the force in the supports—i.e. strain in the wire and the stress in the wire. In terms of previously defined variables, the stress and total strain in the wire are given by

$$\sigma = \frac{F}{A_{\mathrm{SMA}}}, \tag{34}$$

$$\varepsilon = \varepsilon_0 + \frac{\Delta L_{\mathrm{SMA}}}{L^0_{\mathrm{SMA}}} = \varepsilon_0 + \frac{L_{\mathrm{SMA}} - L^0_{\mathrm{SMA}}}{L^0_{\mathrm{SMA}}}, \tag{35}$$

where $A_{\mathrm{SMA}}$ is the SMA wire cross section area, and $\Delta L_{\mathrm{SMA}}$, $L_{\mathrm{SMA}}$, and $L^0_{\mathrm{SMA}}$ are, respectively, the change in length, current length, and length of the SMA wire just after it has been deformed to initial strain level $\varepsilon_0$. From the kinematics developed previously,

$$\Delta L_{\mathrm{SMA}} = L_{\mathrm{SMA}} - L^0_{\mathrm{SMA}} = |\vec{R}_F(x_s, y_s) - \vec{R}_F(-x_s, -y_s)| - |\vec{R}_F(x_s, y_s) - \vec{R}_F(-x_s, -y_s)|_{F=0}, \tag{36}$$

where, recall, $\vec{R}_F$ is the position vector to the tip of the support, where the wire is attached and the force is applied. Thus, the strain in the SMA wire can be expressed by

$$\varepsilon = \varepsilon_0 + \left( \frac{|\vec{R}_F(x_s, y_s) - \vec{R}_F(-x_s, -y_s)|}{|\vec{R}_F(x_s, y_s) - \vec{R}_F(-x_s, -y_s)|_{F=0}} - 1 \right). \tag{37}$$

The deformations of the laminate can be predicted as a function of the temperature in the SMA wire by solving the above set of equations in conjunction with Eq. (22), which governs the laminate behavior. When the SMA wire is heated above the austenite start temperature, the wire starts to contract, stress is generated in the wire, which results in applying a force $F$ on the laminate. The force $F$ is induced by the phase transformation and is therefore not known in advance.

One way to solve the equations would be to use an iterative process, as Boyd and Lagoudas (1996) did. In that case, values are assumed for the temperature and the total strain in the wire and Eqs. (33), (27) and (25) can be evaluated to determine the stress in the wire. Using Eq. (34), the force $F$ applied on the laminate is obtained and the coefficients $c_i$, $i = 1, \ldots, 14$, for the plate response may be computed by solving Eq. (22). From the values for coefficients $c_i$, $i = 1, \ldots, 14$, $\vec{R}_F$ can be evaluated. Substituting these values into Eq. (37), a new value for the total strain in the SMA wire can be computed. The same computations with Eqs. (33), (27), (25), (34), and (22) are performed another time with the new value for the total strain. This procedure should be followed until the value computed for the total strain has converged.

Another way of solving the equations consists in assuming values for the force $F$ generated by the SMA wire and using the governing equations for the laminate and the SMA wire to compute the corresponding plate response, strain in the wire, martensite volume fraction, and temperature in the wire. This procedure has the advantage of being quick to perform since no iteration is required. Therefore, it will be used to

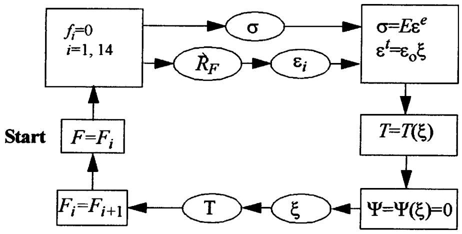


Fig. 7. Description of the computation process.

predict the laminate deformations as a function of the temperature in the SMA wire. The computation scheme is presented in Fig. 7.

Assuming a value for the force $F$ induced by the SMA wire and applied on the laminate, the coefficients $c_i$, $i = 1, \ldots, 14$, for the plate response are computed by solving Eq. (22). From the values for coefficients $c_i$, $i = 1, \ldots, 14$, $\vec{R}_F$ can be evaluated. Substituting the value for $\vec{R}_F$ into Eq. (37), the total strain in the SMA wire, $\varepsilon$, is computed. Moreover, using Eq. (34), the stress in the SMA wire, $\sigma$, is determined from the force $F$. Substituting Eq. (27) and the values obtained for $\sigma$ and $\varepsilon$ into Eq. (25), the temperature in the wire, $T$, is determined as a function of the martensite volume fraction, $\xi$. Substituting this expression into Eq. (33), the nonlinear equation $\Psi = 0$ can be solved for the martensite volume fraction. The temperature in the wire can then be evaluated. Using *Mathematica* by Wolfram (1991), this computation process is performed for every increase in the applied force. For the calculations, the properties of the SMA wire are taken to be

$$\begin{aligned}
&E_A = 9.710 \text{ Ksi}, \qquad C_A = 1.104 \text{ Ksi}/°F, \\
&E_M = 3.810 \text{ Ksi}, \qquad A_{s0} = 94.3 \text{ °F}, \\
&a_A = 19.8 \times 10^{-6} \text{ °F}^{-1}, \qquad A_{f0} = 120.2 \text{ °F}, \\
&a_M = 11.88 \times 10^{-6} \text{ °F}^{-1}, \qquad A_{\text{SMA}} = (\pi d^2)/4, \\
&\varepsilon_0 = 8\% \text{ (maximum)}, \qquad d = 20 \times 10^{-3} \text{ in.}
\end{aligned} \tag{38}$$

All values of the material parameters are based on manufacturer's data. The diameter $d$ of the wire was measured. Attention now turns to application of the model.

## 4. Comparison of numerical results with experiments

### 4.1. Experimental considerations

When using SMA wire with highly curved unsymmetric laminates, several important issues, as previously mentioned, have to be considered. First, the SMA wire should be attached on the laminate close enough to its surface so that the recovery strain needed to make the laminate snap does not exceed the maximum recovery strain, which, as stated in Eq. (38), is 8% for the material used here. That is, the longer the supports, the more strain must be recovered in the wire as a result of the curvature of the laminate decreasing from point $C$ to point $G$ in, for example, the upper portion of Fig. 4. However, the supports to which the SMA wire is attached should be long enough so the SMA wire does not touch the laminate. The laminate can be snapped even if the wire touches the laminate, but the analysis is complicated beyond that which was developed in the previous sections. The issue is to find a good combination for $L_s$ and $e$ (see Fig. 3) which satisfies the strain recovery and the geometric no-touch conditions. Since the cross-ply laminate exhibits the largest curvature, this laminate will require the largest SMA strain recovery when compared to the other laminates. Therefore, the $[90_4/0_4]_T$ laminate is a good case for determining the design of the wire support geometry.

The second issue to consider is the moment level necessary for snapping. As was seen in Figs. 4 and 5, the moment level needed for snapping depends on the laminate family and on the layer fiber angles, $\Theta$, within the family. Also, as discussed in connection with Eqs. (31)–(33), the SMA wires can become saturated before the necessary moment level is achieved. Obviously, the moment level depends on the force level and the support length. With constraints on the support length due to the recovery strain level and the no-touch conditions, attention then focuses on the force level achievable. As the $[90_4/0_4]_T$ laminate requires the most moment to produce snapping, this laminate can also be used to determine the maximum force level requirements. The key issue is knowing how much force can be generated by a single SMA wire in the context of this particular experiment. If a single wire is not enough, then multiple wires, in parallel, can be used. The force level achievable from a single wire can be determined from a theoretical standpoint by using the parameters of Eq. (38). However, it was felt best here to conduct a simpler experiment with a single SMA wire to determine the force level that could be generated. In that spirit, an initial experiment was conducted using a flat narrow aluminum plate with two supports and a single SMA wire. The idea was to heat the SMA wire and deform the aluminum plate, comparing the measured deformations with the predictions of the model simplified to represent the aluminum plate. Besides being able to measure achievable force levels, the aluminum plate experiment provided an opportunity to conduct an experiment without the complication of material anisotropy, test the computational scheme on a simpler example, further develop the experimental concepts, and possibly refine some of the parameters of the SMA wire relative to the manufacturer's nominal values. The section to follow describes the aluminum plate experiment and the comparisons with model predictions.

### 4.2. Aluminum plate

The aluminum plate experiment was based on a plate with dimensions $L_x = 20.75$ in., $L_y = 3.00$ in., and $H = 0.0625$ in., where the nomenclature of Fig. 3a is being used. The supports were located symmetrically relative to the geometric center of the plate such that $x_s = 9.75$ in. and $y_s = 0$. Also, for the supports, $e = 0.625$ in. and they were made of steel. The SMA wire was given an initial strain of $\varepsilon_0 = 5\%$ and was stretched between the supports. A strain level of 5% was used, rather than the maximum stated by the manufacturer of 8%, to provide some degree of latitude, if needed. Two thermocouples measured the wire temperature (two so as to have measurements at two different locations along the length of the wire), and back-to-back strain gages, mounted parallel to the long direction of the plate, measured plate response. The SMA wire was heated progressively by slowly increasing the voltage. For each voltage increment, the temperature in the wire and the strains in the plate were measured. As the austenitic start temperature was reached, the phase transformation occurred quite fast. As the voltage was further increased, the strains in the plate increased, then reached a stationary value, indicating that the phase transformation process was over. Figure 8a shows the plate before voltage was applied to the SMA wire, and Fig. 8b shows the plate in the state of maximum deflection (note that the voltage is nonzero in Fig. 8b). Though not clear in the photograph, because of the electrically conducting properties of aluminum, the supports were electrically insulated from the plate by using nylon spacers between the plate and the base of the supports. Nylon bolts were used to attach the supports to the plate.

The strains measured as a function of temperature are represented in Figs. 9a and b. Predictions of the model are also indicated in the figures, where the value of the extensional modulus for aluminum was assumed to be $10^7$ psi and Poisson's ratio was taken to be 0.3. As the wire was heated from room temperature, the strains remained close to zero. After the temperature reached about 86 °F, the strains started increasing. When the temperature equaled 140 °F, the strains stop increasing and remain constant, even though the SMA wire continued to be heated. The dashed line shows the predictions of the model using the

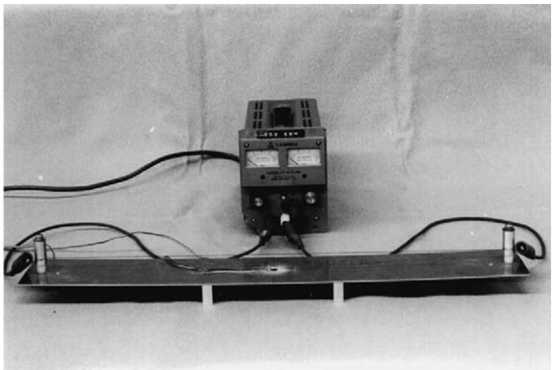

(a) Before voltage is applied

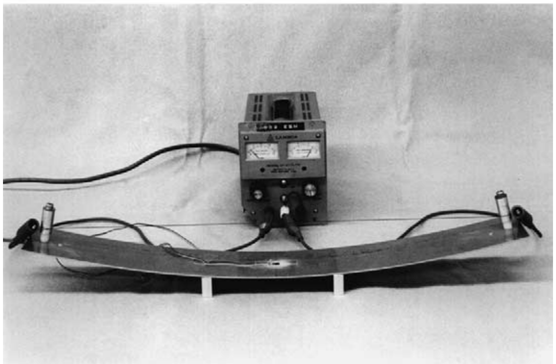

(b) after SMA wire has saturated with strain

Fig. 8. Aluminum plate experiment.

manufacturer's material parameters, in particular, the values of $A_{s0}$ and $A_{f0}$. It can be observed that the austenitic start temperature $A_{s0}$ was actually much less than the value of 94.3 °F used in the prediction. Furthermore, the rate of increase of the measured strains was quite different than predicted. Using a simple method of trial and error, it was found that using 100.4 °F for $A_{f0}$ and 77.0 °F for $A_{s0}$ in the model gave predictions which were quite close to the experimental measurements, as illustrated in the figures by the solid line. Calculations showed that a reasonable working level of achievable force for a single SMA wire was 13 lb.

From the results of the aluminum plate experiment, it appeared that the constitutive model of Boyd and Lagoudas (1996) adequately represented the behavior of SMA wire within the context of usage in the study. The SMA model would be used with a degree of confidence with unsymmetric laminates. This is the subject of the next section.

### *4.3. Unsymmetric laminates*

Using the force level of 13 lb, the fact that from Fig. 4 the moment required to snap the $[90_4/0_4]_T$ laminate is equal to about 30 lb–in., considering the initial curvature of the $[90_4/0_4]_T$ and the desire to not have the SMA wire touch the laminate, and considering a recovery strain level of 5%, it was decided to use four parallel wires for the $[90_4/0_4]_T$ laminate to produce the snap-through. The geometric parameters of the supports were taken to be

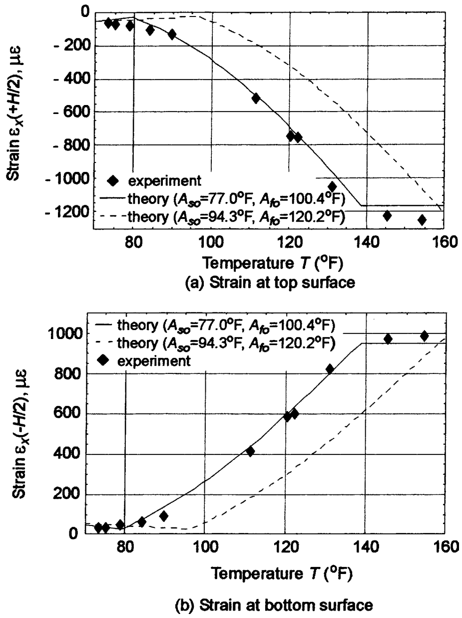


Fig. 9. Comparison of strain measurements with predictions.

$$L_s = 4.0 \text{ in.}, \qquad e = 0.625 \text{ in.} \tag{39}$$

For the $[90_4/0_4]_T$ laminate, this meant $x_s = 4.0$ in. and $y_s = 0$. To reduce the number of variables in the experiment, these values of $L_s$ and $e$ were used for the other unsymmetric laminates considered, and the number of wires was changed according to moment needed to snap the laminate.

The scheme to use multiple parallel wires is described in more detail in Fig. 10. Figure 10a is a schematic of four separate wires in parallel. The problem with this arrangement is that all four wires needed to be stretched between their supports with the same slight initial tension, or one wire would contribute more to the applied moment than the other, and possibly become saturated with stress before the other wires did. To overcome this problem, the arrangement shown in Fig. 10b, which employed just one continuous wire, was used. The one continuous wire was attached to end supports and looped around so-called sliding supports. The sliding supports were designed so the wire could slide around them, the result being that the slight initial tension in the wire was the same along its entire length. As the wire contracted due to actuation through a temperature increase, the developed force was distributed evenly among the four lengths of wire. Figure 11 shows the support configuration of the multiple lengths of wire for the four laminates tested.

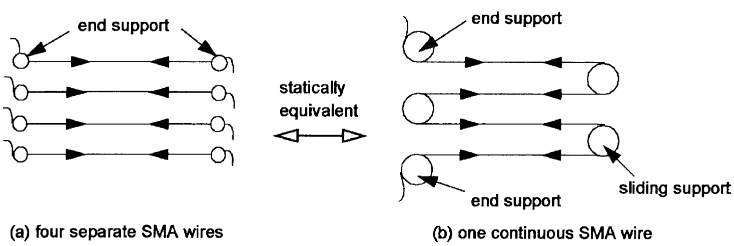


Fig. 10. SMA wire attachment.

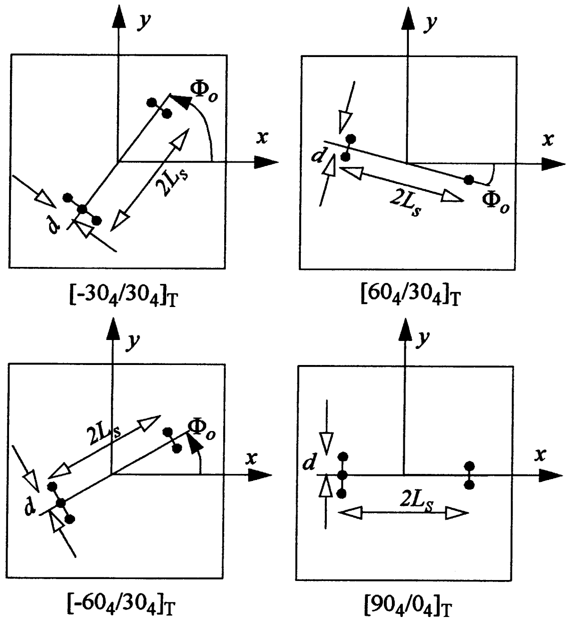


Fig. 11. General configuration of supports for multiple wire arrangement.

As can be seen, the $[-30_4/30_4]_T$, $[-60_4/30_4]_T$, and $[90_4/0_4]_T$ laminates used four parallel lengths, while the $[60_4/30_4]_T$ laminate used only two lengths. Though the geometry of the two and four length arrangements did not exactly coincide with the geometry of the single force and two supports shown in Figs. 2 and 3, and assumed in the subsequent theory developed, the net effects of the multiple lengths of wire were felt to be a reasonable approximation to the effects of a single wire. The results in Figs. 4 and 5 and the results of the aluminum plate experiment were used to determine the number of parallel wires needed.

As examples of the unsymmetric laminates with the SMA wires attached, Fig. 12a shows the $[90_4/0_4]_T$ laminate and Fig. 12b shows the $[-60_4/30_4]_T$ laminate, both made of graphite-epoxy. The sliding supports are the shorter supports. As with the aluminum plates, because of the electrically conducting properties of the graphite fiber, the steel supports were electrically insulated from the laminates by using nylon spacers between the laminate and the base of the supports, and nylon bolts to attach the supports to the laminate. The nylon spacers are the light colored section at the base of each support. Also seen in the photographs are the leads for the back-to-back 0–45–90 strain gage rosettes which were used to measure the strain response of the laminates. Ideally, the displacements or curvatures of the laminate as a function of wire temperature would have been measured. These responses, however, are difficult to measure because of the large displacements involved. The strain response was easier to measure and was used as an indicator of laminate response. As graphite-epoxy is dark in color, before curing, light-colored Kevlar™ fibers were laid at intervals in the $x$- and $y$-directions to form a grid to make it easier to see the deformations of the darker graphite-epoxy laminates. The dimensions of the laminates were as in Figs. 4 and 5, namely, $L_x = L_y = 11.5$ in.

In the figures to follow, the relationship between the SMA wire temperature and the measured and predicted strains is plotted. For each unsymmetric laminate the tests were conducted twice, and the results of both tests will be shown. It should be mentioned that in the figures to follow, the differences between the predicted and measured curvatures of the laminate at room-temperature conditions, such as shown in Fig. 12, were negligible. The shapes of unsymmetric laminates can change with time due to moisture absorption

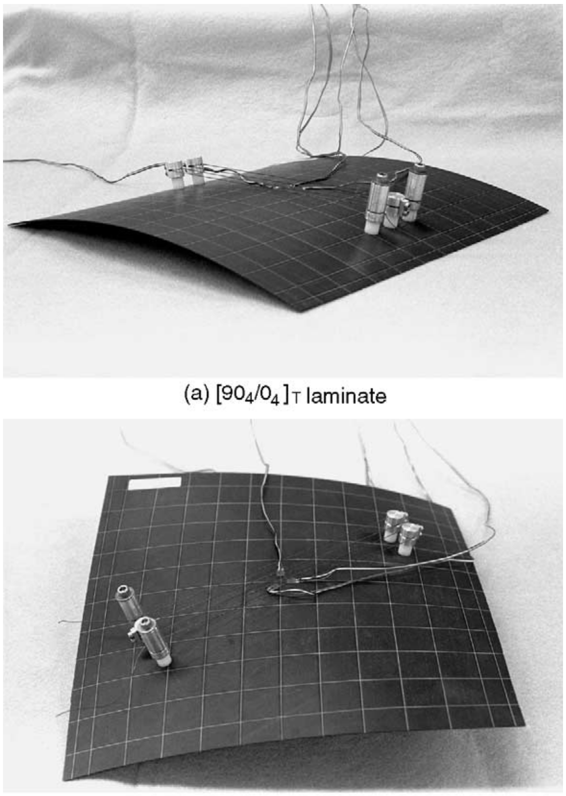

(a) $[90_4/0_4]_T$ laminate

(b) $[-60_4/30_4]_T$ laminate

Fig. 12. Photographs of laminates with SMA wire and supports.

and relaxation effects in the epoxy. The former effect can be reversed by heating the laminate at a temperature somewhat above room temperature for 24–48 h prior to use to cause desorption of the moisture. The latter effect is permanent, but can be accounted for by assuming the cure temperature to be somewhat lower than that actually used. For example, instead of using $\Delta T$ equal to −280 °F to represent the change in temperature from cure conditions to room temperature, $\Delta T$ can be assumed to be −260 °F to reflect a lower stress-free temperature. The predicted and measure room-temperature curvatures can be matched quite accurately with this technique.

#### 4.3.1. $[-30_4/30_4]_T$ laminate

As can be observed in Fig. 13, for both test 1 and test 2, the measured strains for the $[-30_4/30_4]_T$ laminate changed very slowly, or not at all, as the SMA wire was first heated above the room temperature start condition. The predictions also indicated a slow change. As the SMA wire was further heated, the rate of change of the measured strains with increasing temperature remained slow for both tests, while the predictions indicated that the strains should change more rapidly. At a temperature of 104 °F for test 1, the laminate snapped, as characterized by a sudden jump in the strains. The strain along the 45°-axis, $\varepsilon_{45}$, changed the most before the snap-through because, compared to the $x$- and $y$-axes, the 45°-axis was the closest to one principal curvature direction, along which the strains underwent the largest change due to snap-through. After snapping, the strains on the top surface ($z = +H/2$) were all negative, since the top

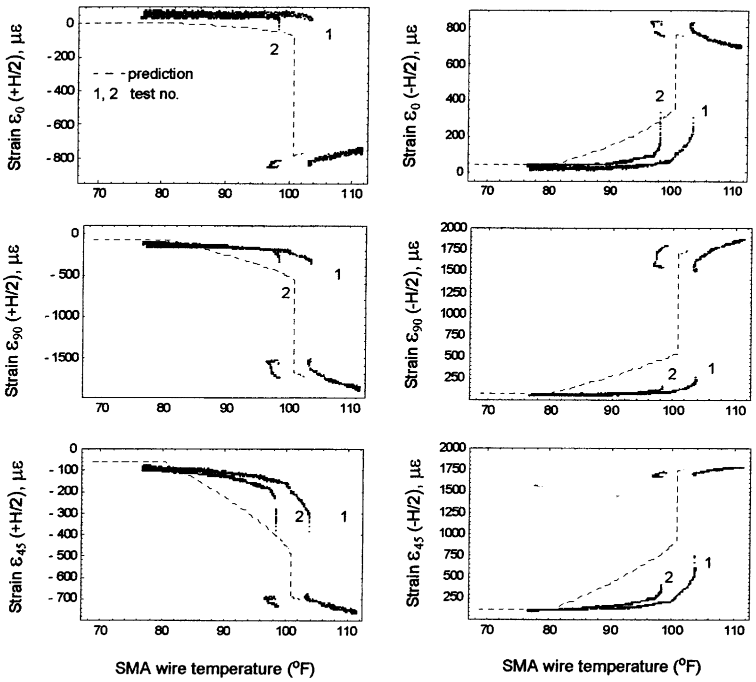


Fig. 13. SMA wire temperature–laminate strain relations: $[-30_4/30_4]_T$ laminate.

surface was being compressed when the force was applied. The strains on the bottom surface ($z = -H/2$) were all positive. These signs were consistent with the direction of the SMA-induced curvature change in Figs. 2–5. Similar characteristics can be described for test 2, except snapping occurred at a temperature of 98.6 °F, 5.40 °F lower than test 1. Despite this 5.40 °F difference, the average snapping temperature for the two tests was close to the predicted value.

The predicted pre-snap-through strain levels were close to the measured values, and for a given gage location, the pre-snap-through strain levels for both tests were similar. For example, just prior to snap-through, the 45° gage on the top surface measured about −400 με for both tests, and the prediction was about −450 με, not a bad comparison. Just after snap-through, that same gage registered about −680 με for both tests, and the theory predicted about −690 με. Similar comparisons just before and just after snap-through can be made for most gages. As mentioned above, it was how the strains reached the pre-snap-through levels as a function of temperature that was not well predicted. With increasing temperature from the room-temperature start condition, the measured strains did not change much, then suddenly changed at the snap-through temperature. In contrast, after 82.4 °F the prediction indicated the strains should have increased steadily until snap-through. It is believed much of this discrepancy was due to the lack of flexibility in the model. In the experiments, a considerable part of the laminate deformations due to the SMA forces could have taken place locally at the base of the support until the forces were large enough to cause snap-through. Then the overall deformation level changed suddenly. With the supports attached basically at a point, this could have easily been the case. The model, on the other hand, was based on three curvature parameters, namely $c_9$, $c_{10}$ and $c_{11}$ in Eq. (6), that were assumed to be valid over the entire laminate, not just in the center, where the strain gages were mounted, nor just at the base of the supports, where the force was being transmitted into the laminate. It is also felt that the nylon insulators at the base of the supports and the nylon bolts for attaching the supports may have contributed to local flexibility of the support. Nylon is soft compared to the steel of the supports.

#### 4.3.2. $[60_4/30_4]_T$ laminate

The results for the $[60_4/30_4]_T$ laminate are shown in Fig. 14. Of the four unsymmetric laminates tested, this laminate showed the poorest correlation between experiments and predictions. Like the $[-30_4/30_4]_T$ laminate, the measured strains did not change as rapidly with temperature from the room-temperature start condition as the predicted strains. The strain gages in the 0°-direction exhibited the largest change just before snap-through because the principal curvature direction was close to the 0°-direction. The temperature at snap-through for test 1 was about 96.8 °F, while for test 2 it was about 100.4 °F, representing a 3.60 °F difference. The predicted snap-through temperature did not compare well with the average measured snap-through temperature. However, for a given strain gage location and for both tests, the strain levels just before snap-through were very similar, e.g., −425 for $\varepsilon_0(+H/2)$, and for both tests the laminate snapped to very similar strain levels, e.g., −650 for $\varepsilon_0(+H/2)$. The aforementioned flexibility of the laminate and support system, as compared to the model, influenced the rate of change of strain with temperature, but it is not clear why the strain levels and the snapping temperature predicted did not correlate well with the measurements.

#### 4.3.3. $[-60_4/30_4]_T$ laminate

The results for the $[-60_4/30_4]_T$ laminate are shown in Fig. 15. The results from test 1 and test 2 agree quite well with each other in all respects, except the snap-through temperature for test 1 was 109.4 °F, while for test 2 it was 106.4 °F. These results were close to the predicted snap-through temperature. The predicted strain levels just before snap-through do not agree well with either measurement.

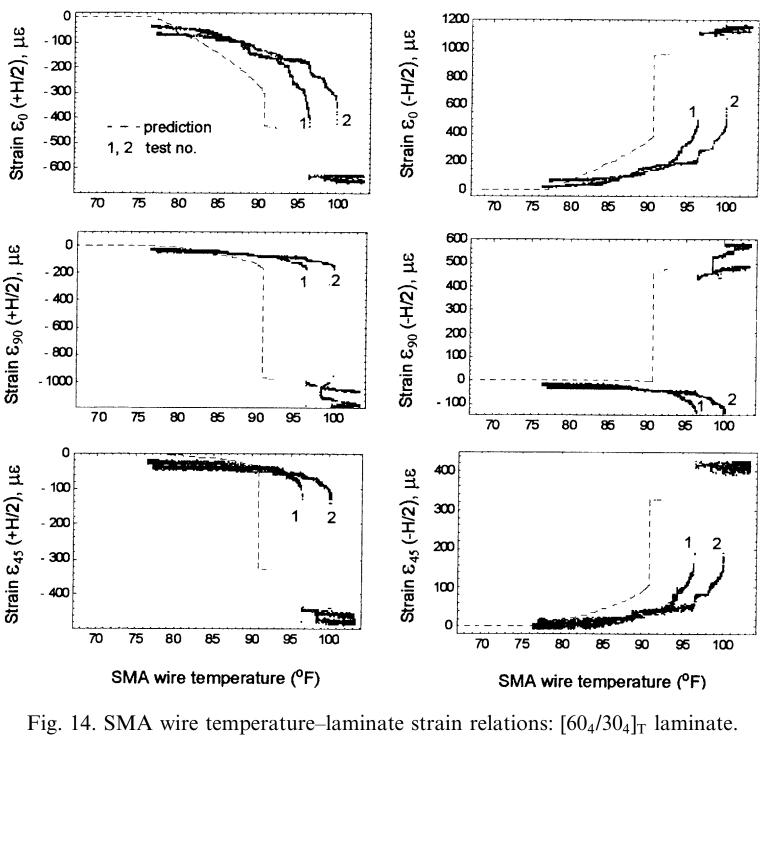


Fig. 14. SMA wire temperature–laminate strain relations: $[60_4/30_4]_T$ laminate.

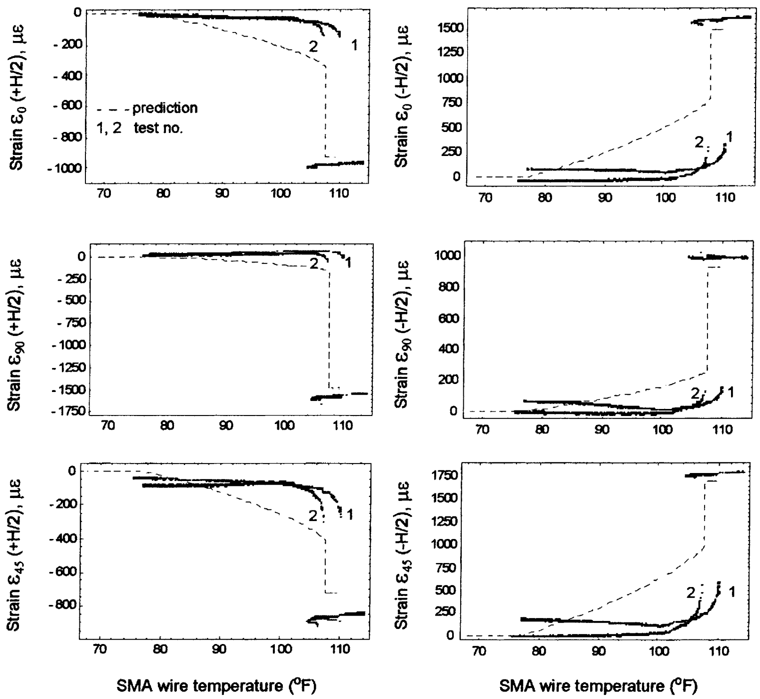


Fig. 15. SMA wire temperature–laminate strain relations: $[-60_4/30_4]_T$ laminate.

### 4.3.4. $[90_4/0_4]_T$ laminate

The results for the $[90_4/0_4]_T$ laminate are shown in Fig. 16. Again, the results from test 1 and test 2 are in agreement with each other and, except for the rate of change of strain with temperature, with the predictions. The snap-through temperature for test 1 was 107.6 °F and for test 2 it was 105.8 °F. The predicted snap-through temperature was somewhat higher than either test value. With a few exceptions, the measured levels of strain before and after snap-through were in agreement with the predictions. The reasonable correlation for this case was gratifying because, as mentioned earlier, the forces required for snap-through were the greatest, and the deformations were the greatest, which could have had a bearing on whether or not the strain in the SMA wire was within the margin of the recovery level.

## 5. Discussion

The results for the four laminates tested provide clear evidence that the concept considered works and, to within a reasonable level of agreement, the equations governing the behavior of the two important components, namely, the unsymmetric laminate and the SMA wires, represent the physics. The lack of better agreement, however, is troubling. One important issue with this particular experiment was achieving no slack, but very little initial tension, in the SMA wire as it was being attached to the supports. The laminate would deform slightly under even small forces on the supports, and care had to be taken to keep the initial deformations and initial forces to a minimum. The strain gages on the laminate were used to some extent to monitor initial laminate deformations due to initial tension in the wire, but they could not monitor initial slack in the wire. Any initial slack would have to be taken up before the wire would generate force on the supports, and this would require a temperature increase not contributing to laminate deformations.

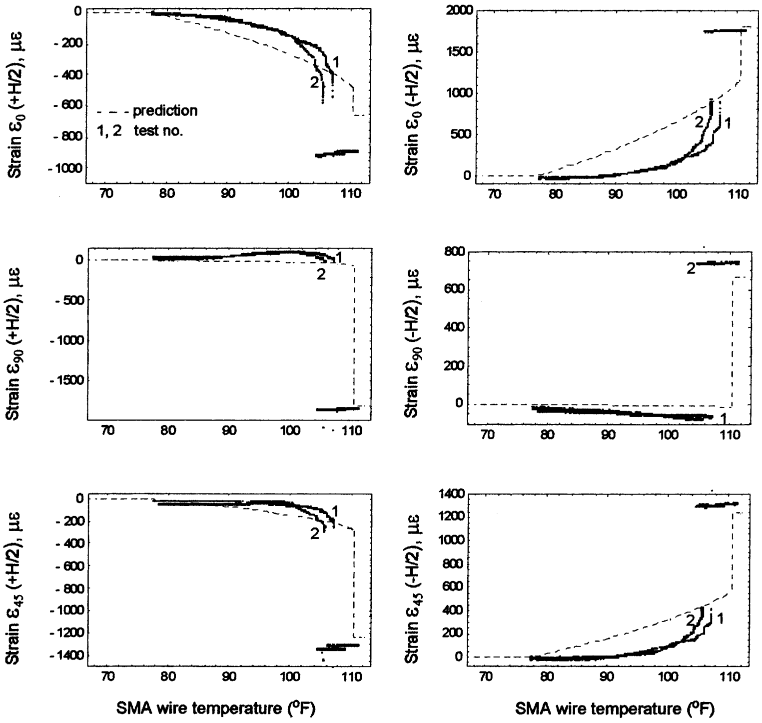


Fig. 16. SMA wire temperature–laminate strain relations: $[90_4/0_4]_T$ laminate.

As another factor, the same single length of SMA wire was used throughout, and it was the one used with the aluminum plate. Perhaps a new length of wire should have been used for each laminate. It was an issue of knowing the calibration of the specific length of wire by way of the aluminum plate experiment vs. possible aging effects due to the repeated use of the same length of SMA wire. As was seen with the four laminates discussed here, there did not seem to be a trend that resulted in, for example, the test 2 snapping temperature always being greater or less than the test 1 snapping temperature. Any aging effect due to repeated usage was not in evidence in this regard. Another aspect to consider is the fact that the snap-through of the laminate is a dynamic and unstable event, which can be influenced by small unwanted perturbations. This may be responsible to some extent for the differences noticed between the two tests. Finally, it is important to keep in mind that the analysis proposed to predict the laminate behavior is a global-level analysis, based on the assumptions that the curvatures are constant throughout the laminate. However, the forces induced by the SMA cause the laminate to deform locally at the base of the supports rather than deform uniformly over the entire laminate, so there is not as much strain produced at the center of the laminate where the strain gages are mounted as there is near the supports. As a result, the rate of change of the measured strains with increasing temperature is slower than predicted. A similar phenomenon was observed by Dano and Hyer (2002) when studying the snap-though of unsymmetric laminates. A finite-element analysis may be able to predict more accurately the laminate deformations, but such an analysis was beyond the scope of this study.

## 6. Summary and conclusions

This paper explored the concept of using SMA wires to change the equilibrium configuration of unsymmetric laminates. An approximate theory has been presented to predict the snap-through of unsymmetric laminates induced by SMA wires. The laminate mechanical behavior was predicted by a theory based on assumed strain and displacement fields, the Rayleigh–Ritz technique, and virtual work. The equations governing the laminate behavior were coupled to equations governing the SMA wire behavior. The snap-through characteristics of the laminate were predicted as a function of the temperature in the SMA wire by solving the set of coupled equations. Experiments that were used to calibrate the model and to study SMA-induced deformations in four unsymmetric laminates were described. Laminate strain levels vs. temperature in the wire were measured for these laminates. The experimental results showed good repeatability and were in reasonable agreement with the predictions.

From the results of this investigation, it is can be concluded that it is possible to use SMA wires to change the shape of unsymmetric laminates, and to predict reasonably well the overall response of the laminate as a function of the SMA wire temperature. As stated at the onset, it was not the intent of the work discussed to address all issues related to the concept, but rather to study the important mechanics issues and establish that the overall idea is feasible. Based on what was presented, that has been done. It would seem that future efforts would focus on refining the concept, perhaps, as alluded to in Section 1, adding a similar support and SMA wire arrangement on the opposite side of the laminate to effect the reverse snap, and to make the wire and support system more tidy. Other topics can be listed.

## Acknowledgements

This work was supported, in part, by funds from Grant NAG-1-343 from the NASA-Langley Research Center, Dr. James H. Starnes, Jr., monitor, and from the Virginia Tech Center for Composite Materials and Structures. Both authors express their appreciation for the support.

## References

Boyd, J.G., Lagoudas, D.C., 1996. Thermodynamical constitutive model for shape memory materials, Part I: The monolithic shape memory alloy. Int. J. Plast. 12 (6), 805–842.

Cho, M., Kim, M.-H., Choi, H.S., Chung, H.C., Ahn, K.-J., Eom, Y.S., 1998. A study on the room-temperature curvature shapes of unsymmetric laminates including edge effects. J. Compos. Mater. 32 (5), 460–482.

Dano, M.-L., Hyer, M.W., 1996. The response of unsymmetric laminates to simple applied forces. Mech. Compos. Mater. Struct. 3, 65–80.

Dano, M.-L., Hyer, M.W., 1997. Thermally-induced deformation behavior of unsymmetric laminates. Int. J. Solids Struct. 35 (17), 2101–2120.

Dano, M.-L., Hyer, M.W., 2002. Snap-through behavior of unsymmetric fiber-reinforced composite laminates. Int. J. Solids Struct. 39, 175–198.

Hamamoto, A., Hyer, M.W., 1987. Non-linear temperature-curvature relationships for unsymmetric graphite epoxy laminates. Int. J. Solids Struct. 23 (7), 919–935.

Hyer, M.W., 1981a. Some observations on the cured shapes of thin unsymmetric laminates. J. Compos. Mater. 15, 175–194.

Hyer, M.W., 1981b. Calculations of the room-temperature shapes of unsymmetric laminates. J. Compos. Mater. 15, 296–310.

Hyer, M.W., 1982. The room-temperature shapes of four-layer unsymmetric cross-ply laminates. J. Compos. Mater. 16, 318–340.

Hyer, M.W., 1998. Stress Analysis of Fiber-Reinforced Composite Materials. WCB/McGraw-Hill, New York, NY. pp. 212–347.

Jun, W.J., Hong, C.S., 1990. Effect of residual shear strain on the cured shape of unsymmetric cross-ply thin laminates. J. Compos. Sci. Technol. 38, 55–67.

Jun, W.J., Hong, C.S., 1992. Cured shape of unsymmetric laminates with arbitrary lay-up angles. J. Reinf. Plast. Compos. 11 (12), 1352–1366.

Peeters, L.J.B., Powell, P.C., Warnet, L., 1996. Thermally-induced shapes of unsymmetric laminates. J. Compos. Mater. 30 (5), 603–626.

Schlecht, M., Schulte, K., 1999. Advanced calculations of the room-temperature shapes of unsymmetric laminates. J. Compos. Mater. 33 (16), 1472–1490.

Schlecht, M., Schulte, K., Hyer, M.W., 1995. Advanced calculations of the room-temperature shapes of thin unsymmetric composite laminates. Compos. Struct. 32, 627–633.

Tuttle, M.E., Koehler, R.T., Keren, D., 1996. Controlling thermal stresses in composites by means of fiber prestress. J. Compos. Mater. 30 (4), 486–502.

Wolfram, S., 1991. Mathematica: A System for Doing Mathematics by Computer. Addison-Wesley Publishing Co., Redwood City, CA.